

See discussions, stats, and author profiles for this publication at: <https://www.researchgate.net/publication/325963958>

The Dynamic Response of a Pinhole Microphone under Flows of Varying Shear Stress

Conference Paper · June 2018

DOI: 10.2514/6.2018-3933

CITATIONS

4

READS

299

4 authors, including:



N. Agastya Balantrapu

University of Utah

13 PUBLICATIONS 63 CITATIONS

SEE PROFILE



Liselle Joseph

Virginia Tech (Virginia Polytechnic Institute and State University)

14 PUBLICATIONS 114 CITATIONS

SEE PROFILE



William Devenport

Virginia Tech (Virginia Polytechnic Institute and State University)

335 PUBLICATIONS 5,349 CITATIONS

SEE PROFILE



The Dynamic Response of a Pinhole Microphone under Flows of Varying Shear Stress

N. Agastya Balantrapu*, Russell J Repasky†, Liselle A Joseph‡, and William J Devenport.§
Center for Renewable Energy and Aerodynamic Technology (CREATE)
Virginia Tech, Blacksburg, VA, 24060

Measurements have been made to document the effects of mean shear on the dynamic response of pressure field microphones with a pinhole cap designed for the measurement of wall pressure fluctuations in turbulent flows. Experiments were performed using B&K 4138 1/8th inch microphones with 0.5 and 0.35-mm diameter pinholes, under a boundary layer with edge velocities up to 60 m/s, which implies a maximum wall shear stress of approximately 10-N/m². An increase in the resonant frequency of the microphone-pinhole combination and some reduction in the associated damping were observed with increases in flow speed.

I. Introduction

PRESSURE fluctuations beneath turbulent boundary layers have been the focus of many research efforts due to their scientific and engineering significance. Understanding the nature of these pressure fluctuations has the potential to add to the fundamental understanding of the workings of the turbulent boundary layer, particularly the regions closest to the wall. Furthermore, since the pressure fluctuations are the source of unwanted structural vibrations and acoustic noise, it is of engineering interest to be able to reliably predict the pressure spectrum.

Many of the past works in this field have been experimental in nature, commonly utilizing microphones as pressure sensors at the wall beneath the flow. These microphones are almost always outfitted with pinhole caps in order to reduce the sensing area thereby minimizing spatial averaging. This is particularly important in high Reynolds number flows, where the range of scales is quite large, which are of most practical interest. The works of Schewe⁵ and Gravante *et al.*⁶ have proposed criteria based on both pinhole diameter and flow conditions. In this way, experimenters are able to ascertain the frequencies above which attenuation is significant based on the experiment. These advances have improved the study of pressure spectra and allows researchers to remove artifacts of the microphone response characteristics from the actual flow behavior.

However, artificially reducing the effective sensor size also affects the dynamic response of the microphone. The addition of the pinhole cap forms a cavity between the microphone diaphragm and the sensing area, which effectively converts the microphone into a Helmholtz resonator. Figure 1 shows a schematic of the situation. The pressure at the wall of the flow p can be determined from the pressure sensed in the cavity (p_m) using a one-dimensional momentum balance. The mass of vibrating air through the pinhole is excited by the pressure difference between the cavity and the ambient ($p_m - p$) acting over the pinhole area A and constrained by conservation of mass in the cavity. The motion is opposed by frictional resistance assumed to be proportional to the vibration velocity u_2 with a coefficient RA , where R is the acoustic resistance. Solving the momentum balance results in Eq. (1):

$$\frac{\hat{p}_m}{\hat{p}} = \frac{1}{-\omega^2 \frac{L_{eff} V}{c_0^2 A} + i\omega \frac{RV}{\rho_0 c_0^2 A} + 1} \quad (1)$$

where ρ_0 and c_0 are the ambient density and sound speed and the equation is written for harmonic fluctuations of the form $p = \hat{p}e^{i\omega t}$. The pinhole cavity thus behaves as a second order system. The resistance and the inertia terms can

* Graduate Research Assistant, Department of Aerospace and Ocean Engineering, AIAA Student Member.

† Graduate Research Assistant, Department of Aerospace and Ocean Engineering, AIAA Student Member.

‡ Graduate Research Assistant, Department of Aerospace and Ocean Engineering, AIAA Student Member.

§ Professor, Department of Aerospace and Ocean Engineering, AIAA Associate Fellow.

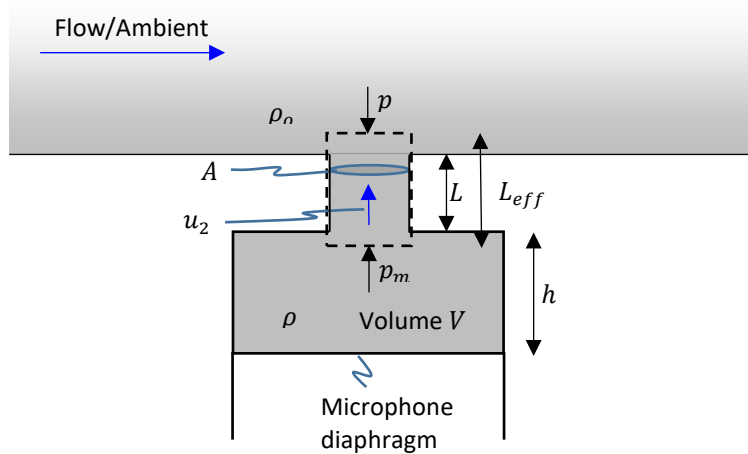


Figure 1: Schematic introducing the nomenclature view of the Helmholtz Resonator formed by the pinhole aperture and the cavity, from Glegg and Devenport¹

be lumped into a single acoustic impedance $Z = R + i\chi$ where the reactance $\chi = \rho_0 L_{eff} \omega$. The effective depth of the pinhole L_{eff} is greater than the geometric value L due to additional flow above and below the aperture. For a zero-mean flow and a circular pinhole that is shallow compared to its diameter d , potential flow modelling⁷ indicates that $L_{eff} = \pi d/4$, suggesting that L_{eff} may be modified to $L + \pi d/4$ when the depth is significant. Other similar end corrections exist, see particularly Ingard⁸. The acoustic resistance R of the system is dependent on the situation and, at low cavity sound pressure levels where linear viscous effects on the orifice walls and corners dominate, can be taken as^{9, 10}:

$$R = \rho_0 \sqrt{8\nu\omega} (1 + L/d) \quad (2)$$

where ν is the kinematic viscosity of the air.

This effect on the dynamic response of the pinhole microphone is well known and often calibrated out of measured pressure spectra^{2, 11-13}. This typically involves estimating the transfer function of the pinhole microphone when exposed to a white noise source in a quiescent medium with a zero mean flow. The resulting transfer function enables in principle the removal of the resonant peak from measured pressure spectra. However, this removal is not always perfect. Meyers *et al.*¹³ and Joseph¹⁴ carried out experiments using pinhole microphones to measure the pressure fluctuations in a high-Reynolds number turbulent boundary layer. Calibrations for the dynamic response of the pinhole microphones were carried out as described above. However, subsequent measurements of turbulent wall pressure fluctuation spectra showed resonant peaks slightly different than observed in the quiescent calibration, the difference becoming particularly apparent at flow speeds over 30 m/s. It was proposed that the grazing flow over the phase of the microphone was the cause of changes in the response of the Helmholtz-resonator system within the pinhole cavity. Specifically, one would expect the high velocity gradient at the wall, characterized to be the wall shear stress, to be the dominant controlling factor.

The influence of grazing flows over Helmholtz resonators and orifices has been extensively studied in the past because of its relevance to aircraft engine liners, automobile silencers and other noise control applications. Research has been particularly focused on non-linear effects associated with losses due to jetting of the unsteady flow through the orifice. Studies have included flow visualization and detailed flow measurements¹⁵⁻¹⁸, pressure measurements using cavity backed orifices exposed to flow^{3, 19-21} and a number of modeling and computational efforts^{9, 22-24}. These efforts have included studies of multiple orifices (perforate) with reference to many liner and silencer configurations. Generally these authors have shown that grazing flow increases acoustic resistance and reduces reactance, equivalent to a reduction in the effective orifice depth. While these studies have been concerned with grazing flow conditions similar to those of the present work, they have generally be concerned with orifices and cavities at least an order of magnitude larger than that of a typical pinhole microphone, and of quite different configuration. Fig. 2 is a scaled drawing of one of the pinhole microphones of interest to the present study. By design, the cavity is particularly short

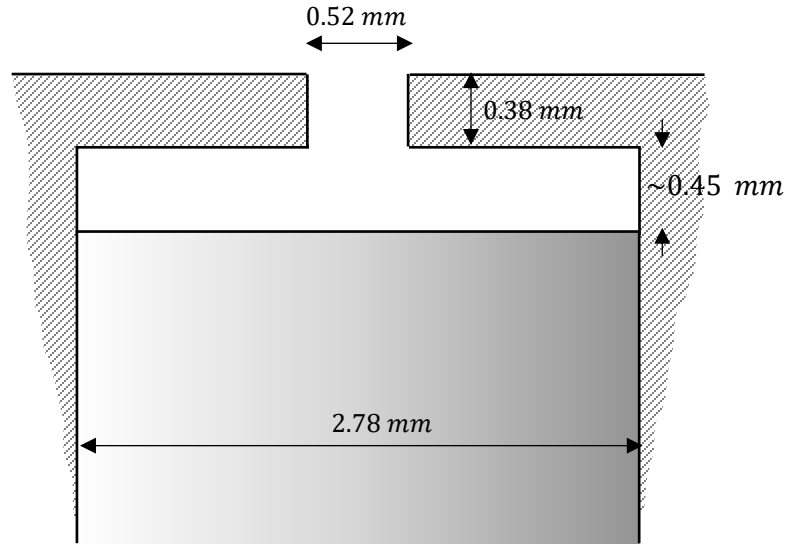


Figure 2: Scale drawing of microphone configuration 1 and measured dimensions.

compared to other applications since this reduces its volume and increases its resonant frequency to minimize its impact on the frequency range of turbulent pressure fluctuations. As a result the cavity height is of the order of the pinhole diameter and this likely influences both viscous losses and the effective pinhole depth.

To correct for the effect of grazing flow shear stress on the microphone response, Meyers *et al.*¹³ and Joseph² adopted a method of optimizing the calibration during post-processing by iteratively adjusting the constants in the second-order transfer function used to curve fit the calibration so as to match the resonant peak observed in boundary layer measurements. This method, while effective and apparently robust, suffers from the shortcoming that it is not fully independent of the measured wall pressure spectrum. The purpose of the present work is therefore to directly study this effect. Our aim is to characterize the effect of changes in shear stress at the aperture of the pinhole microphone on the dynamic response of that system. The ultimate goal is to uncover a generalized relationship between the flow conditions, the physical dimensions of the pinhole cap, and the changes in the system dynamics that can be applied *a priori* in the measurement of turbulent wall pressure fluctuations.

II. Apparatus and Instrumentation

Dynamic calibrations, using a white noise source, were performed on a series of microphone configurations installed in the wall of a wall-jet wind tunnel over which a turbulent boundary layer is growing. To ensure success, the white noise source was set up to be loud enough to be clearly audible above the boundary layer's pressure fluctuations. From the perspective of minimizing flow-induced pressure fluctuations and being able to readily evaluate the shear stress, a laminar boundary layer would have been preferable for this experiment. However, the preliminary work of Joseph² showed that the shear within a laminar boundary layer was insufficient in producing the dynamic effects on the microphone response which are the subject of this investigation.

A. Pinhole Microphones

Bruel & Kjaer (B&K) 4138-A-015 1/8-in microphones were studied in combination with three different pinholes. The 4138 is a pressure-field microphones optimized to have a flat frequency response from 6.5 Hz - 140 kHz and a dynamic range of 168 dB in its unmodified state. The sensitivity of this microphone is nominally 1 mV/Pa. The 4138 is supplied with a screw-on 'salt and pepper shaker' cap for normal use (Fig. 3a). B&K supplied additional blank caps, identical in terms of their mounting and external dimensions, in which a pinhole could be drilled (Fig. 3b). A total of 5 microphone configurations were the subject of the present experiments, as

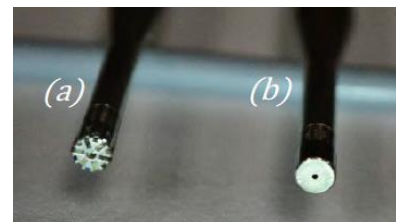


Figure 3: B&K 4138 with (a) factory-supplied salt and pepper shaker cap and (b) pinhole cap.²

detailed in Table 1. Three microphones (numbered 4, 1 and 3) were studied in combination with three pinholes (A through C) with two different nominal diameters (0.5 mm and 0.35 mm).

Configuration	Mic	Pinhole	d	L	h
1	4	A	0.51	0.38	0.45
2	1	B	0.52	0.32	0.38
3	3	B	0.52	0.32	0.36
4	1	C	0.35	0.33	0.40
5	3	C	0.35	0.33	0.45

Table 1: Measured characteristics of the microphone configurations. Dimensions in millimeters.

Table 1 includes measured dimensions of the 5 microphone configurations. Configuration 1 (pictured in Fig. 2) used microphone 4 in combination with 0.51-mm diameter 0.38-mm deep pinhole A. The cavity diameter D , assumed identical for all mic configurations, was measured on configuration 1 as 2.78 mm. The measured cavity depth h of 0.45 mm implies a cylindrical volume of 2.75 mm^3 , i.e. ignoring possible regions at the edge of the cavity where the cap makes contact with the microphone capsule. Further uncertainty in the volume comes from uncertainty in the measurement of h which involved microphone disassembly and optical measurements from an unfavorable angle. Configurations 2 and 3 used microphones 1 and 3 and nominally identical pinhole cap B with a pinhole diameter of 0.52 mm and slightly smaller depth of 0.32 mm. Configurations 4 and 5 re-use microphones 1 and 3 but with a 0.35-mm wide 0.33-mm deep pinhole.

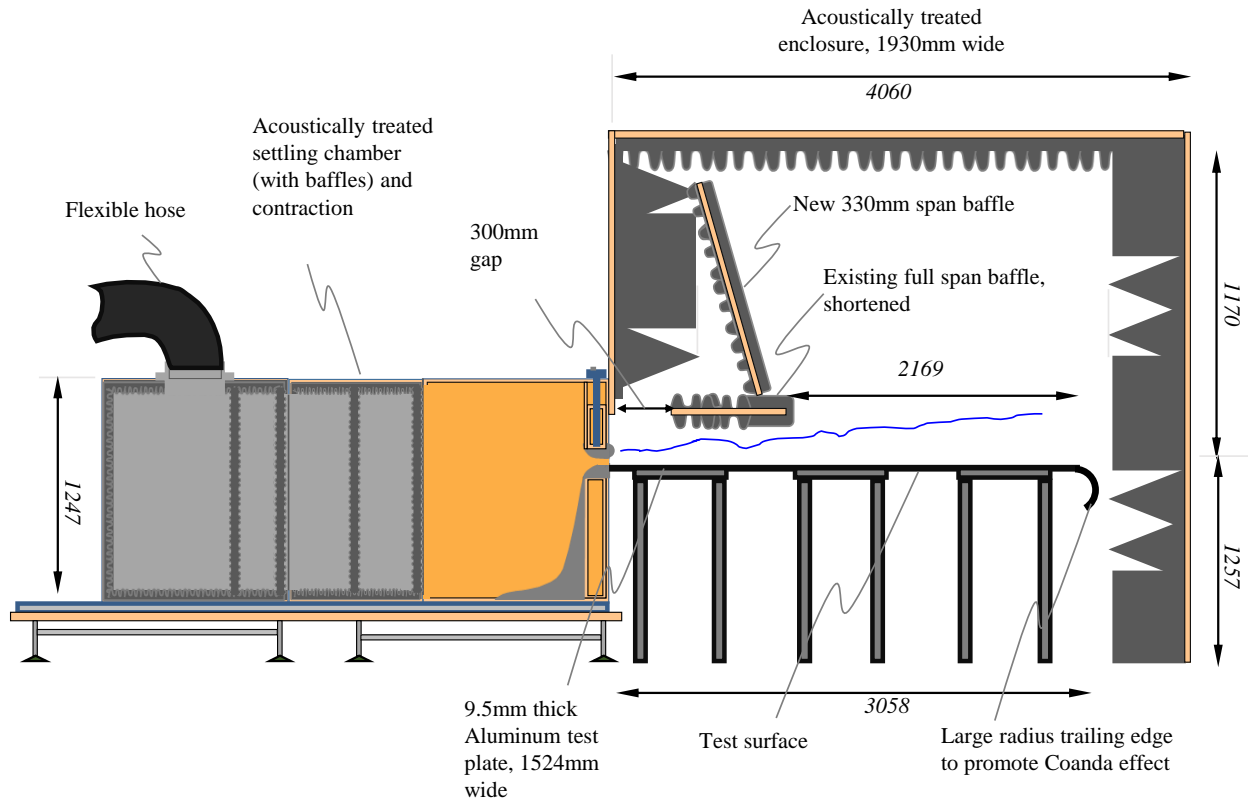


Figure 4: Side-view schematic of the Virginia Tech Anechoic Wall Jet Wind Tunnel. All dimensions shown are in mm. Adapted from ⁴

B. Wall-Jet Facility, Instrumentation and Test Setup

Experiments were conducted in the Virginia Tech Wall-Jet facility, Fig. 4. This facility produces a 2-dimensional stream of air which exhausts tangentially onto a flat plate. This facility was upgraded during the course of this research so that some measurements were made before the renovation while others after. However, unless otherwise noted, the facility characteristics were the consistent between both sets of experiments.

Air is driven by a centrifugal fan via a flexible hose pipe into an acoustically treated settling chamber. This air then accelerates through a nozzle, 1219 mm wide and 12.7 mm in height, and exhausts onto a smooth flat aluminum plate, 3 m long and 2 m wide. The nozzle and the aluminum plate are contained in an acoustically treated chamber. As the wall-jet travels downstream, an inner boundary layer and an external mixing layer develop. These eventually merge to form a fully developed wall-jet flow. Experiments were made by mounting the microphone in the wall jet plate close to the nozzle where the boundary layer was thin and still structurally distinct from the mixing layer.

In configuration 1, measurements were made with the microphone placed close to the spanwise center of the plate 175 mm downstream of the nozzle exit. In this case the boundary layer was tripped 16-mm downstream of the nozzle exit using 12-mm wide and 0.5-mm thick Glasfaser-Flugzeug-Service GmbH 3-D Turbulator tape. A second reference B&K 4138 microphone without pinhole was mounted in the wall displaced spanwise 13-mm from the test microphone. White noise was generated by a University Sound ID60C8 speaker placed out of the flow, with its outlet 62-mm above the wall and centered between the microphones. Cross-spectra between each of the microphone signals and the white noise signal to the speaker were measured and then divided to infer the dynamic calibration of the microphone with pinhole. The assumptions here are, of course, that the dynamic calibration of the unmodified reference microphone was not affected by its placement or the flow, and that the sound field received by the two microphones was the same. The latter assumption was verified by switching the microphone positions and repeating measurements.

For configurations 2 through 5 the same basic arrangement was used in the renovated wall jet facility, the key differences being that (a) the microphones were placed 171 mm downstream of the nozzle, (b) the boundary layer was not tripped since calculations showed it would undergo natural transition upstream of the trip location in any case, and c) the speaker was positioned 51 mm above the microphones to reduce sound interference patterns.

The flow speed at the nozzle exit, assumed equal to the edge velocity of the boundary layer at the measurement location, was varied from 0 to 60 m/s and sensed from the difference in the total pressure in the settling chamber and the static pressure in the test-section. The pressure differential was measured to within $\pm 0.14\%$ (full-scale) using a Setra 239 Pressure transducer with a range of ± 3.25 kPa. A thermocouple placed at the spanwise end of the nozzle exit was used sense flow temperature. With this instrumentation the flow speed could be determined to $\pm 2.4\%$ at 20 m/s and $\pm 0.6\%$ at 60 m/s²⁵. Wall shear stress at the measurement locations was estimated using a finite difference boundary layer calculation. For both facility setups the friction velocity U_τ was found to vary from 4.9% of the boundary layer edge velocity U_e at $U_e = 20$ m/s to 4.6% of U_e at $U_e = 60$ m/s implying a maximum wall shear

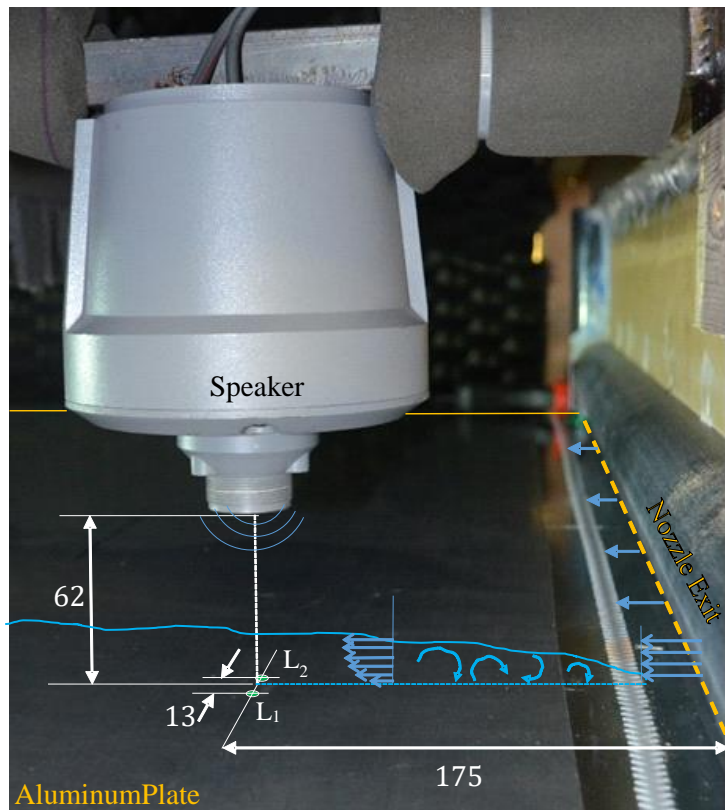


Figure 5: Photographic view of the experimental set-up for configuration w featuring the test-section with tripped inflow, microphone locations L_1 , L_2 and white-noise speaker. All dimensions shown are in mm.

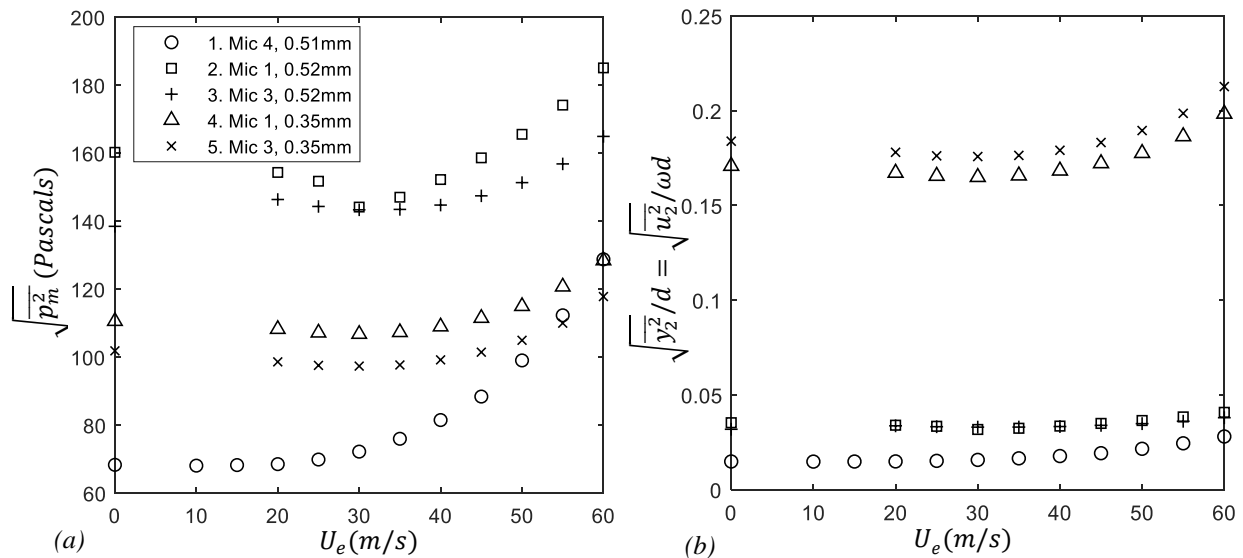


Figure 6: Overall sound levels recorded by the test microphone for each configuration and flow speed. (a) RMS levels. (b) Levels interpreted in terms of motion in the pinhole.

stress of close to $10 N/m$. These results were taken to indicate that the edge velocity could be used as a satisfactory proxy for the friction velocity in analyzing the microphone results.

Microphones were operated by and measurements digitized using a B&K LAN-XI 24-bit DAQ system sampling at 65536 Hz. For each measurement 120 seconds of data were collected continuously, processed in records of 8192 consecutive samples. The speaker volume was adjusted based on a subjective assessment of the signal to noise ratio needed to overcome contamination from boundary layer pressure fluctuations. Fig. 6 shows the total mean square pressure recorded by the subject microphone for each configuration and speed. Levels were largest for configurations 2 and 3 at around 160 Pa (138dB re. 20 μ Pa), and as low as 67 Pa (131 dB) for low flow speeds with configuration 1.

III. Results and Discussion

A. Calibrations without flow

Fig. 7 shows the dynamic calibrations for the five microphone configurations without flow. The configurations with 0.5-mm pinholes show a resonant peak around 16 kHz and an accompanying increase in phase lag. With the 0.35-mm pinhole resonance occurs around 8 kHz and appears much more damped. These features have been quantitatively analyzed by fitting the calibrations to the form of the theoretical response function of equation 1 with a resistance proportional to the square root of frequency, as in equation 2. Specifically, the model equation is,

$$\frac{p_m}{p} = \frac{1}{-A_1\omega^2 + iA_2\omega^{3/2} + 1} \quad (3)$$

where $A_1 = 1/\omega_r^2$, with ω_r being the resonant frequency, and A_2 represents the frequency independent portion of a normalized viscous damping. Resonant frequencies with no flow are listed in table 1. Mean square errors in these curve fits are 0.010, 0.018, 0.031, 0.009, 0.005 for configurations 1 to 5 respectively. The greater errors for configurations 2 and 3 might be indicative of a more non-linear response at the higher pressure fluctuations levels used in these cases (Fig. 6).

Based on the derivation of equation 1, we would expect the resonant frequency to be related to the physical characteristics of the microphone configuration as,

$$\omega_r = c_0 \sqrt{\frac{A}{L_{eff}V}} \quad (4)$$

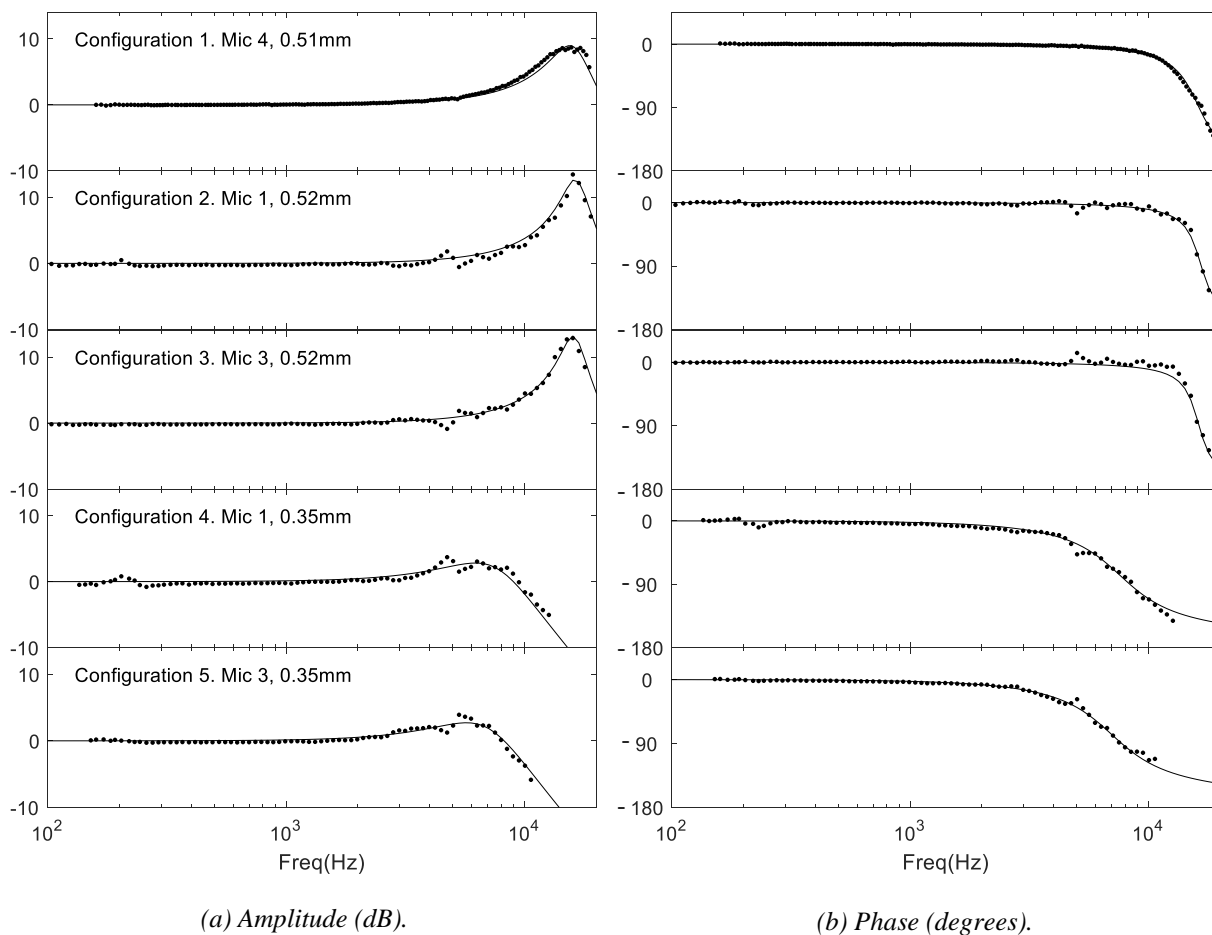


Figure 7: Dynamic response calibrations with no flow. Points – measurements; lines – response model.

For configuration 1, using the known sound speed c_o , the measured dimensions of the pinhole and cavity volume given in Fig. 2, and the effective pinhole depth $L_{eff} = L + \pi d/4$, gives a resonant frequency of about 107,000 rad/s (17 kHz) – surprisingly close to the measured value. This agreement might appear fortuitous since the same calculation for configurations 4 and 5 produces a value 50% greater than the measured values. However, this discrepancy might be due to the uncertainty in the cavity volume described above. Added to this, it is possible that the flexibility of the microphone diaphragm may be a contributor. This flexibility is equivalent to an increase in the cavity volume, if the deflection of the diaphragm (and the additional volume it generates) is proportional to the pressure imposed upon it*. This is the case if deflection of the diaphragm in response to pressure changes is treated as quasi-static²⁶, an assumption which seems reasonable given that the response of the B&K 4138 without pinhole is flat to 140 kHz. To avoid these issues an effective cavity volume V_{eff} for each of the 5 configurations was calculated using the measured resonant frequencies and is presented in Table 2.

* This follows from the relationship between pressure and density in the cavity. We have $\frac{1}{c_o^2} \frac{\partial p_m}{\partial t} = \frac{\partial \rho}{\partial t} = \frac{1}{V} \frac{\partial M_c}{\partial t} - \frac{M_c}{V^2} \frac{\partial V}{\partial t} = -\frac{\rho_o u_2 A}{V} - \frac{\rho_o k}{V} \frac{\partial p_m}{\partial t}$ where M_c is the mass of air in the cavity and k is the constant of proportionality between pressure on the diaphragm and volume change. Thus we have $\left(\frac{1}{c_o^2} + \frac{\rho_o k}{V}\right) \frac{\partial p_m}{\partial t} = -\frac{\rho_o u_2 A}{V}$ or $\frac{1}{c_o^2} \frac{\partial p_m}{\partial t} = -\frac{\rho_o u_2 A}{V_{eff}}$ where the effective cavity volume $V_{eff} = V + \rho_o c_o^2 k$.

Configuration.	ω_r (rad/s)	V_{eff} (mm ³)	$\sqrt{y_2}$ (mm)	$\frac{\sqrt{y_2}}{L}$	$\sqrt{u_2}$ at ω_r (m/s)	$\frac{\sqrt{u_2}L}{v}$	$\frac{R/\sqrt{\omega}}{\rho_0\sqrt{\omega_r}L_{eff}}$	
							From A_2	From eqn 2
1	102100	3.01	7.59E-03	0.020	0.78	18	0.37	0.080
2	104378	3.20	1.84E-02	0.058	1.92	37	0.23	0.079
3	102133	3.35	1.66E-02	0.052	1.70	32	0.22	0.080
4	52373	6.92	5.98E-02	0.181	3.13	63	0.89	0.161
5	48440	8.09	6.44E-02	0.195	3.12	63	0.90	0.167

Table 2: Characteristics of the microphone configurations inferred from no-flow dynamic calibrations.

The RMS amplitude of the fluid motion in the pinholes can be estimated from the RMS pressure in the cavity by conservation of mass as

$$\sqrt{y_2^2} = \frac{V_{eff}}{\rho_0 c_0^2 A} \sqrt{p_m^2} \quad (5)$$

Values for $\sqrt{y_2^2}$ are given in Table 1 (absolute, and normalized on pinhole depth), and in Fig. 6(b) (normalized on pinhole diameter). For the case of no flow, this value varies from a minimum of about 8 microns (2% of the pinhole depth) for configuration 1, through about 17 microns (5 to 6%) for configurations 2 and 3, to about 60 microns (18-19% of the pinhole depth) for the 0.35-mm pinhole configurations 4 and 5 (Table 2). Multiplying by angular frequency to get RMS velocity amplitude in the pinholes implies Reynolds numbers based on pinhole diameter of about 18, 35 and 63, respectively, at resonance.

The coefficient A_2 in the model equation representing the viscous damping is related to the non-dimensional acoustic resistance as

$$A_2 \omega_r^{3/2} = \frac{R/\sqrt{\omega}}{\rho_0 \sqrt{\omega_r} L_{eff}} \quad (6)$$

Values of $\frac{R/\sqrt{\omega}}{\rho_0 \sqrt{\omega_r} L_{eff}}$ inferred from the curve fits (Table 2) are 3 to 5 times those obtained from equation 2. The largest discrepancies are associated with the 0.35-mm pinhole cases which might be due to the non-linear effects associated with the larger pinhole velocities. The viscous losses associated with flow over the center of the microphone diaphragm beneath the pinhole may be an additional source of discrepancy.

B. The effects of flow

Dynamic calibrations were performed at flow speeds up to 60m/s, implying pinhole diameters in terms of wall units ($d^+ = dU_\tau/\nu$) up to 85 for the 0.5-mm pinholes and 59 for the 0.35-mm pinholes. Fig. 8 shows measured dynamic calibrations for configuration 1 as a function of boundary layer edge velocity. There is clearly a shear effect. The resonant frequency appears to increase slightly with flow speed and the resonant peak narrows, as if the damping were reducing. This is not what would be expected from most prior work on Helmholtz resonators with grazing flow, where most researchers have shown an increase in resistance with flow speed. However, these authors have generally been concerned with larger and therefore higher Reynolds number, configurations.

There is no particular reason to believe that the model form of equation 3 would be physically correct in the presence of grazing flow. Therefore, a number of alternative functional forms were investigated, inspired by corrections proposed by previous researchers. Forms which did not allow adjustment with speed of the reactance were quickly disregarded because these could not adequately fit the observed variations. Among the various forms used to model the resistance term (e.g. fixing a viscous component according to equation 2, or at its value measured without grazing flow, and allowing a non-frequency dependent term), none could fit the measured calibrations with better subjective and mean-square accuracy than equation 3. The only exception was a fit allowing for independent

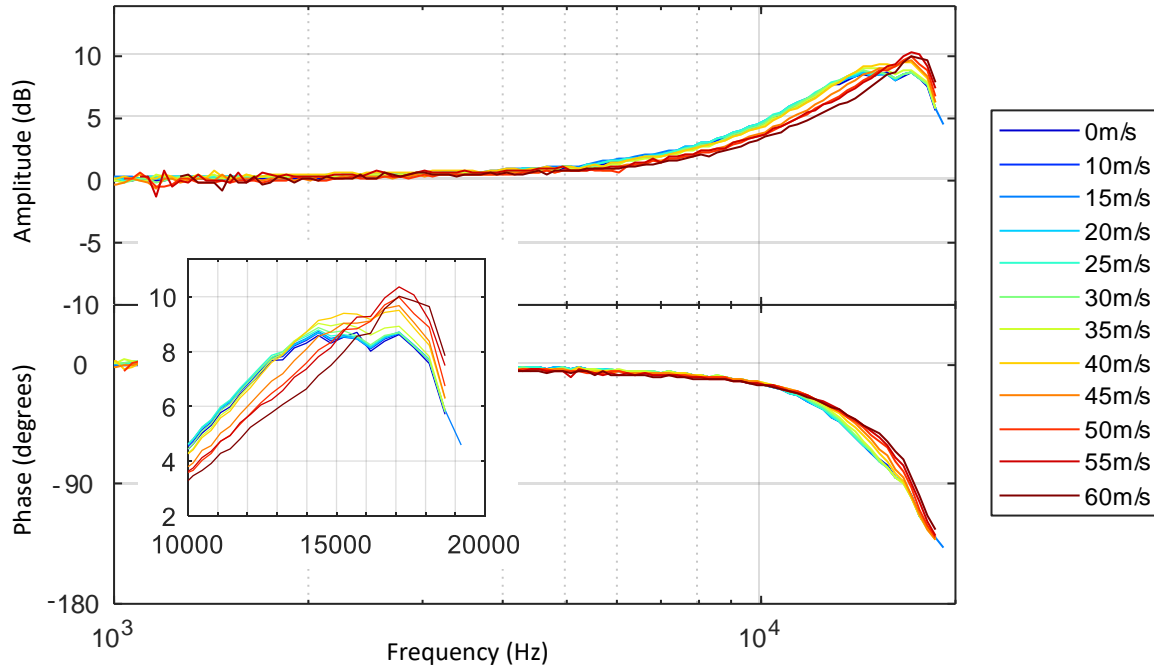


Figure 8: Measured dynamic response calibrations as a function of flow speed. Inset shows detail of amplitude response in the vicinity of the resonant peak.

coefficients multiplying $i\omega^{3/2}$ and $i\omega$ terms, but the dependence of these coefficients was not systematic with grazing flow speed or speed-dependent parameters, suggesting that such a model over specifies the problem.

From equations 3 and 4, we have that the coefficient A_1 represents the resonant frequency so that the square of the ratio of A_1 to its no flow value gives the proportionate change in L_{eff} :

$$\left(\frac{A_1}{A_1|_{U_e=0}} \right)^2 = \frac{L_{eff}}{L_{eff}|_{U_e=0}} \quad (6)$$

Likewise, the combination of equations 6 and 4 yields

$$\left(\frac{A_2}{A_2|_{U_e=0}} \right)^2 = \frac{R}{R|_{U_e=0}} \quad (7)$$

Fig. 9 shows these ratios plotted against dimensional flow velocity for each of the five configurations. The effective orifice depth shows a systematic variation with flow speed that is similar for all the microphone configurations. Specifically, Fig. 9(a) shows that L_{eff} first rises slightly as the flow speed is increased from zero reaching a shallow maximum of about 2% over the no-flow value at 25m/s. The effective depth then falls rapidly reaching 10 to 20% below its no-flow value at 55m/s. The resistance (Fig. 9(b)) also shows systematic dependence on flow speed but significant differences in the scales of that dependence with configuration. For the 0.5-mm pinhole (configurations 1 to 3), the resistance barely changes until the speed is increased above 25 m/s at which point it starts to rapidly drop reaching a minimum of about 85% of its no-flow value around 50m/s. For the 0.35-mm pinhole (configurations 4 and 5) a dip is also seen as the velocity is increased, but it is much shallower reaching a minimum only 5% below the no-flow resistance at about 30 m/s. A drop in resistance is occasionally cited in the literature. Dickey *et al.*³ note a slight decrease in resistance with flow speed below the no-flow value for $0 < U_\tau\omega/d \lesssim 0.04$. Denayer *et al.*²⁷ also note a reduction in resistance in their simulations of a Helmholtz resonator. Negative resistance values relative to the no-flow value have also been discussed²³ as resulting from oscillation of the shear layer over the orifice, generating sound.

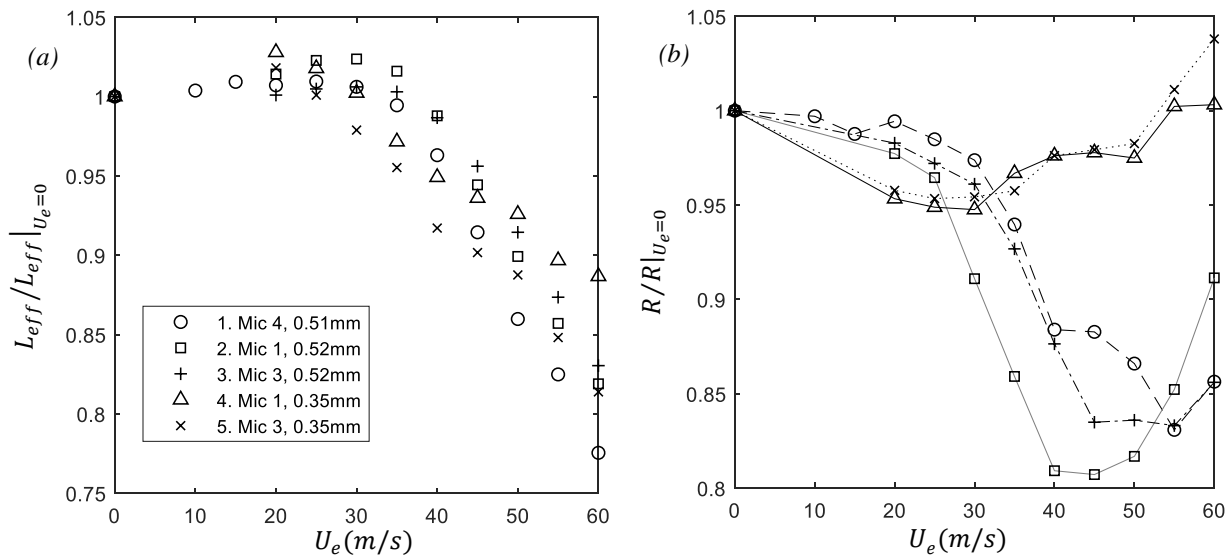


Figure 9: Values of effective pinhole depth and resistance normalized on no flow values as a function of grazing flow velocity.

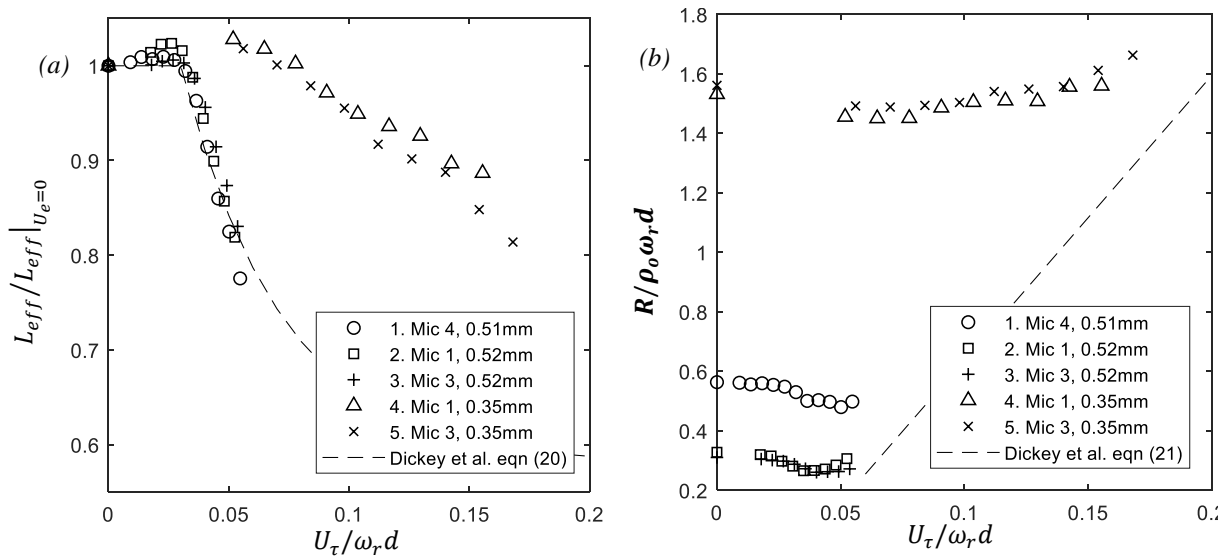


Figure 10: Values of effective pinhole depth and resistance a function of grazing flow velocity plotted using normalizations based on those of Dickey *et al.*³.

However, the resonance peaks of the present calibrations are all at frequencies well above those at which flow induced oscillations might occur²⁸.

Fig. 10 shows these same data but plotted as $L_{eff}/L_{eff}|_{U_e=0}$ and $R/\rho_0 \omega_r d$ against velocity expressed as $U_\tau/\omega_r d$. These are the normalizations of Dickey *et al.*³, but with frequency ω replaced with the resonant frequency ω_r . We believe this is an appropriate substitution since the broadband calibration fitting procedure employed in the present work ensures that resistance parameters will be determined by the response behavior around resonance.

This change of coordinates separates the effective cavity depth variations (Fig. 10(a)) by pinhole size, the results for the 0.35-mm pinhole appearing at much higher $U_\tau/\omega_r d$ values than those for the 0.5-mm pinhole. The 0.5-mm data are quite closely predicted by the curve Dickey *et al.* used to represent their own results. The fact that this curve does not account for the change in pinhole diameter may derive from the fact that Dickey *et al.* established their

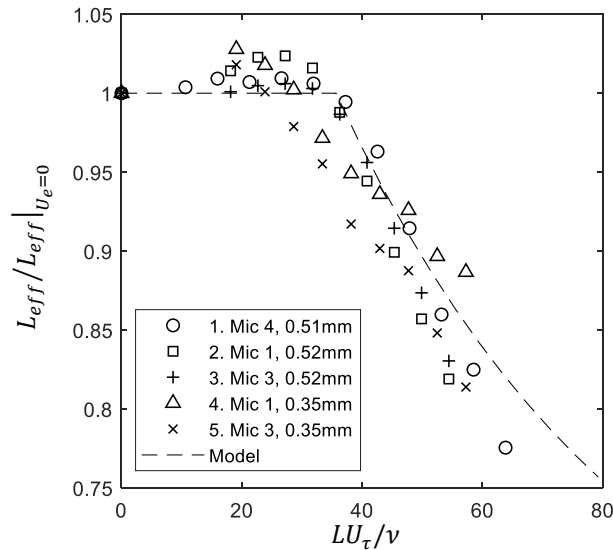


Figure 11: Values of effective pinhole depth a function of grazing flow velocity plotted in terms of cavity depth Reynolds number. Line shows model of Dickey *et al.*³ scaled using configuration 1 results.

correlation using data from a single hole configuration. It is clear from Fig. 9(a) that the normalizing scale for the velocity does not vary much between configuration. One option that awaits physical justification is simply the Reynolds number based on U_τ and the pinhole depth, shown in Fig. 11 and compared with Dickey *et al.*'s curve scaled from Fig. 10(a) using the data from configuration 1.

The normalization $R/\rho_o\omega_r d$ vs. $U_\tau/\omega_r d$ (Fig. 10(b)), certainly does not correlate the resistance data between different configurations. This figure does, however, show the results for the 0.5-mm pinhole cases to fall in the low velocity range where Dickey *et al.* observed slight reductions in resistance. It also highlights how large, relatively speaking, the viscous damping is for the 0.35-mm pinhole configurations. Overall, it appears possible that all the curves might be rising towards the straight line variation that characterized Dickey *et al.*'s results as $U_\tau/\omega_r d$ is increased, though clearly data at higher speeds would be needed to investigate this.

IV. Summary

An experimental study of the velocity dependence of pinhole microphones, used to measure wall pressure fluctuations in turbulent flows, has been performed. Pinhole caps are applied to the B&K 4138 1/8th inch microphones in order to improve their resolution of small scale turbulence. The cap design forms a small Helmholtz resonator above the microphone diaphragm. The dynamic response of this resonator must be measured and accounted for in making turbulence measurements. However, recent results have suggested that this dynamic response is modified by the shear generated by the over-riding turbulent flow, particularly at higher flow velocities. This study has been performed to investigate this phenomenon. The ultimate goal is to uncover a generalized relationship between the flow conditions, the physical dimensions of the pinhole cap, and the changes in the system dynamics that can be applied *a priori* in the measurement of turbulent wall pressure fluctuations.

The dynamic response of 5 microphone configurations, including two different pinhole diameters (0.5-mm and 0.35-mm), were measured as a function of wall shear. The microphones were placed mounted in the surface on which a turbulent boundary layer was growing. A speaker placed outside the flow, above the boundary layer, was used to excite the microphone response with white noise. Measurements were made with boundary layer edge velocities from 0 to 60 m/s. Pressure fluctuations levels measured by the microphone levels (including both the excitation and the boundary layer pressure fluctuations) varied from 131 to 138 dB implying vertical particle motion within the pinholes of between 2% and 19% of the pinhole depth RMS. Dynamic calibrations generated with this procedure were fit to model functions in order to determine the effective reactance and resistance of the configurations.

Small but definite effects of the shear upon the dynamic response characteristics were observed. In accordance with previous researchers studying the response of much larger resonators relevant to liners and silencers, the pinhole microphone reactance was seen to reduce with increase in grazing flow velocity. These changes were interpreted in

terms of a reduction of the effective pinhole depth, by up to about 20% at 60m/s, and an associated increase in the resonant frequency by the same factor. Changes in the effective depth were found to be almost the same for different microphone configurations when normalized on the no-flow value, and plotted against flow velocity. Interestingly, the pinhole microphone resistance was found to first reduce with increasing grazing flow velocity before reaching a minimum. While all microphone configurations showed the same basic dependency, there were clear differences in scale between the 0.35 and 0.5-mm pinholes, the latter showing a much larger reduction, of 15 to 20%, compared to the no-flow value.

Acknowledgments

The authors would like to thank the Office of Naval Research, in particular Drs. Tom Fu, Joe Gorski, and Debbie Nalchajian, for their support under grants N00014-15-1-2247 and N00014-18-1-2179, and the National Science Foundation, in particular Dr. Ron Joslin, for their support under grant CBET-1436088.

References

1. Glegg, S., and Devenport, W. *Aeroacoustics of Low Mach Number Flows: Fundamentals, Analysis, and Measurement*: Academic Press, 2017.
2. Joseph, L. A. "Pressure Fluctuations in a High-Reynolds-Number Turbulent Boundary Layer over Rough Surfaces of Different Configurations," *Aerospace and Ocean Engineering*. Vol. PhD, Virginia Tech, 2017.
3. Dickey, N. S., Selamet, A., and Ciray, M. S. "An experimental study of the impedance of perforated plates with grazing flow," *The Journal of the Acoustical Society of America* Vol. 110, No. 5, 2001, p. 2360.
4. Clark, I. A. "A study of bio-inspired canopies for the reduction of roughness noise." Virginia Tech, 2015.
5. Schewe, G. "On the structure and resolution of wall-pressure fluctuations associated with turbulent boundary-layer flow," *Journal of Fluid Mechanics* Vol. 134, 1983, pp. 311-328.
6. Gravante, S., Naguib, A., Wark, C., and Nagib, H. "Characterization of the pressure fluctuations under a fully developed turbulent boundary layer," *AIAA journal* Vol. 36, No. 10, 1998, pp. 1808-1816.
7. Morse, P. M., and Ingard, K. U. *Theoretical acoustics*: Princeton university press, 1968.
8. Ingard, U. "On the Theory and Design of Acoustic Resonators," *The Journal of the Acoustical Society of America* Vol. 25, No. 6, 1953, pp. 1037-1061.
9. Hersh, A., and Rogers, T. "Fluid mechanical model of the acoustic impedance of small orifices," *2nd Aeroacoustics Conference*. American Institute of Aeronautics and Astronautics, Hampton, VA, 1975.
10. Dickey, N. S., Selamet, A., and Ciray, M. S. "An experimental study of the impedance of perforated plates with grazing flow," *Journal of the Acoustical Society of America* Vol. 110, No. 5, 2001, pp. 2360-2370.
11. Blake, W. K. "Turbulent boundary-layer wall-pressure fluctuations on smooth and rough walls," *Journal of Fluid Mechanics* Vol. 44, No. 4, 1970, pp. 637-660.
12. Varano, N. D. "Fluid Dynamics and Surface Pressure Fluctuations of Turbulent Boundary Layers Over Sparse Roughness," *Aerospace and Ocean Engineering*. Virginia Tech, 2010.
13. Meyers, T., Forest, J. B., and Devenport, W. J. "The wall-pressure spectrum of high-Reynolds-number turbulent boundary-layer flows over rough surfaces," *Journal of Fluid Mechanics* Vol. 768, 2015, pp. 261-293.
14. Joseph, L. A. "Pressure Fluctuations in a High-Reynolds-Number Turbulent Boundary Layer over Rough Surfaces of Different Configurations." Virginia Tech, 2017.
15. Baumeister, K. J., and Rice, E. J. "Visual study of the effect of grazing flow on the oscillatory flow in a resonator orifice," 1975.
16. Baumeister, K. J., and Rice, E. J. "Flow visualization in long-neck Helmholtz resonators with grazing flow," *AIAA Journal* Vol. 16, No. 3, 1978, pp. 233-6.
17. Walker, B. E., and Charwat, A. F. "Correlation Of The Effects Of Grazing Flow On The Impedance Of Helmholtz Resonators," *Journal of the Acoustical Society of America* Vol. 72, No. 2, 1982, pp. 550-555.
18. Charwat, A. F., and Walker, B. E. "The velocity perturbations above the orifice of an acoustically excited cavity in grazing flow," *Journal of Fluid Mechanics* Vol. 128, 1983, pp. 413-26.
19. Cummings, A. "Response Of A Resonator Under A Turbulent Boundary Layer To A High Amplitude Non-Harmonic Sound Field," *Journal of Sound and Vibration* Vol. 115, No. 2, 1987, pp. 321-328.
20. Lee, S.-H., and Ih, J.-G. "Empirical model of the acoustic impedance of a circular orifice in grazing mean flow," *The Journal of the Acoustical Society of America* Vol. 114, No. 1, 2003, pp. 98-113.

21. Hersh, A. S., and Walker, B. E. "Recent advances in resonator physics," *35th International Congress and Exposition on Noise Control Engineering, INTER-NOISE 2006, December 3, 2006 - December 6, 2006*. Vol. 4, Institute of Noise Control Engineering, Honolulu, HI, United states, 2006, pp. 2290-2299.
22. Hersh, A. S., Walker, B. E., and Celano, J. W. "Helmholtz resonator impedance model, part 1: nonlinear behavior," *AIAA Journal* Vol. 41, No. 5, 2003, pp. 795-808.
23. Peat, K. S., Ih, J.-G., and Lee, S.-H. "The acoustic impedance of a circular orifice in grazing mean flow: Comparison with theory," *The Journal of the Acoustical Society of America* Vol. 114, No. 6, 2003, pp. 3076-3086.
24. Selamet, A., and Radavich, P. M. "Helmholtz Resonator: A Multidimensional Analytical, Computational, and Experimental Study." SAE International, 1995.
25. Smith, B. S. "Wall jet boundary layer flows over smooth and rough surfaces." 2008.
26. van der Donk, A. G. H., Scheeper, P. R., Olthuis, W., and Bergveld, P. "Modelling of silicon condenser microphones," *Sensors and Actuators A: Physical* Vol. 40, No. 3, 1994, pp. 203-216.
27. Denayer, H., de Roeck, W., Desmet, W., and Toulorge, T. "Acoustic characterization of a Helmholtz resonator under grazing flow conditions using a hybrid methodology," *19th AIAA/CEAS Aeroacoustics Conference, May 27, 2013 - May 29, 2013*. American Institute of Aeronautics and Astronautics Inc., Berlin, Germany, 2013, p. 74.
28. Alan. Hersh, B. W. "Effect of Grazing Flow on the Acoustic Impedance of Helholtz Resonators Consisting of Single and Clustered orifices," 1979.